

RSC Advances



This article can be cited before page numbers have been issued, to do this please use: D. Panda, A. Nandi, S. K. Datta, H. Saha and S. Majumdar, *RSC Adv.*, 2016, DOI: 10.1039/C6RA06058G.



This is an *Accepted Manuscript*, which has been through the Royal Society of Chemistry peer review process and has been accepted for publication.

Accepted Manuscripts are published online shortly after acceptance, before technical editing, formatting and proof reading. Using this free service, authors can make their results available to the community, in citable form, before we publish the edited article. This *Accepted Manuscript* will be replaced by the edited, formatted and paginated article as soon as this is available.

You can find more information about *Accepted Manuscripts* in the [Information for Authors](#).

Please note that technical editing may introduce minor changes to the text and/or graphics, which may alter content. The journal's standard [Terms & Conditions](#) and the [Ethical guidelines](#) still apply. In no event shall the Royal Society of Chemistry be held responsible for any errors or omissions in this *Accepted Manuscript* or any consequences arising from the use of any information it contains.

Selective Detection of Carbon Monoxide (CO) Gas by Reduced Graphene Oxide (rGO) at Room Temperature

Dipankar Panda, Anupam Nandi, Swapan K. Datta, Hiranmay Saha and Sanhita Majumdar*

*Centre of Excellence for Green Energy and Sensor Systems (CEGESS),
Indian Institute of Engineering Science and Technology (IIST),
Shibpur, Howrah, West Bengal, INDIA*

*Corresponding Author and Address for Correspondence

Dr. Sanhita Majumdar
Centre of Excellence for Green Energy and Sensor Systems (CEGESS)
Indian Institutes of Engineering Science and Technology (IIST)
P.O. Botanic Garden, Shibpur, Howrah, West Bengal, India.
Pin code: 711103.
E-mail: email2sm@gmail.com
Telephone: +91-33-6455-1644
Fax: +91-33-2668-4564

Abstract

Graphene materials have been widely explored for fabrication of gas sensors because of their atom-thick two-dimensional conjugated structures, high conductivity and large specific surface area. Thin graphene layers with attached functional groups desirable for gas sensing applications were synthesized by wet chemical route (modified Hummers' method). Sensing performances of reduced graphene oxide (rGO) against carbon monoxide (CO) were studied in terms of percent sensitivity (sensor response), response and recovery times and I/V characteristics at room temperature as well as at elevated temperatures. Sensitivity data indicate highest activity (~71% sensitivity against 30 ppm CO) at room temperature (RT), indicating that the sensor is best operable at RT. Sensor response is quick (within 30 sec.) even to a trace amount (0.001% or, 10 ppm) of CO gas. Selectivity of the sensor was demonstrated by using different n-type reducing gases (like carbon monoxide, ammonia, methane and hydrogen), at different concentrations, showing negligible sensitivity towards gases other than CO. The synthesized material proves to be good as a selective room temperature sensor for harmful and poisonous carbon-monoxide gas.

Keywords: *Graphene, Gas sensor, Carbon monoxide, Room temperature sensitivity, Selectivity*

Introduction

The use of nanostructured materials in gas detection applications has attracted considerable interest in developing sensors with tailor-made performances. A 2D sheet of sp^2 bonded carbon atoms on a honeycomb lattice, called 'Graphene' has attracted researchers all over the world due to its extra ordinary electronic, mechanical and optical properties since its discovery by Geim and Novoselov in 2004.¹ Graphene has extremely large specific surface area and low electrical noise due to its high degree of crystallinity² making it an ideal material for gas sensor applications. An extremely small change in the resistance of a graphene sheet caused by gas adsorption even down to the molecule level is detectable. The most common source of graphite used for chemical reactions including oxidation, is flake graphite, which is a naturally occurring mineral. Reduced graphene oxide (rGO) or graphene sheets synthesized from such graphite can be processed or assembled into ultrathin sensing layers by a variety of wet techniques such as coating (drop-coat/spin-coat), casting, inkjet-printing, Langmuir–Blodgett technique and layer-by-layer deposition, simplifying the procedures of fabricating gas sensors.³⁻⁴

The first experimental study of graphene for gas sensing was performed by Novoselov et al.¹ They demonstrated the gas-sensing potential of graphene to detect water or ethanol vapors or ammonia gas. However, it was Schedin et al.⁵ who demonstrated that graphene is an ideal material for high sensitive gas detection. Of late, experimental and theoretical assessments of graphene's performance in gas and/or vapor sensing have been made in several reports.⁶⁻⁸

Sensing is a complex function that requires the integration of a number of properties from interface accessibility to transduction efficiency, molecular sensitivity and mechanical or electrical robustness. It appears that graphene fulfills many of these requirements and the realization of highly sensitive graphene sensors could illustrate how the previously described properties can be brought in synergy to this specific objective. Indeed, graphene is a pure interface with almost all atoms exposed to the analyte of interest, since it is only few layers thick.⁹ Moreover, local destruction of the sp^2 lattice preserves its mechanical robustness and does not jeopardize its 2D delocalized transport properties unlike carbon nanotubes. Electronic and mechanical properties can be exploited to perform the transduction of the sensing signal.¹⁰

Since the last few decades, metal oxide based solid state gas sensors are being extensively used, but they suffer from various major drawbacks like poor selectivity, high operating temperatures,

lack of stability etc. High operating temperature restricts their use in remote places. Moreover, high power consumption necessary to achieve high temperature for their operation may cause danger for gases which are flammable/explosive. Poor selectivity makes these sensors unsuitable in places where more than a gas species is available. The aim of the present study was to overcome these problems by using graphene (rGO) as the working material for gas sensors.

Amongst various gases, the detection of CO gas is especially important because it is toxic to humans and other animals. Moreover, being a colorless, odorless and tasteless gas which is slightly less dense than air, it is difficult to recognize in normal way. Carbon monoxide is highly toxic to human beings; the maximum time weighted average (TWA) exposure value or permissible exposure limit ascribed by the United States National Institute of Occupational Safety and Health, is 35 ppm over an 8 h period.¹¹ Inhaling CO over TWA can cause headache, nausea, vomiting, dizziness and fatigue. CO combines irreversibly with hemoglobin (iron-center) of blood and produces carboxy-hemoglobin, which prevents delivery of oxygen to tissues. Thus carbon monoxide is constantly in the public eye, largely because the home is such a susceptible place for carbon monoxide poisoning.

In this work the synthesis of graphene layers by inexpensive wet chemical route (through modified Hummer's method) has been reported with layer thickness of ~2 nm (detected by AFM height profile measurement). The sensing properties of rGO (a non-metal oxide material) are employed for detecting low-concentration of CO gas, under the most practical environment, *viz.*, room temperature and atmospheric pressure, in presence of ambient humidity. Suitable sensing sites have been established through prolonged refluxing. Sensors fabricated using synthesized rGO show as high as 71% sensitivity at room temperature against 30 ppm carbon monoxide gas. Significantly, sensitivity decreases with increasing operating temperature. Low cost fabrication of the device prototype was, thus, feasible.

Experimental

Chemical used

Graphite powder [BurGOyne Urbidges]; H₂SO₄, Sulphuric acid [Merck, Emplura]; KMnO₄, Potassium permanganate [Merck]; H₂O₂, Hydrogen peroxide [Merck]; N₂H₄, Hydrazine hydrate [Sigma Aldrich]. All the chemicals were of analytical reagent grade and used as-received, without further purification.

Wet chemical synthesis by modified Hummers' method

Graphite powder (1g; particle size $\sim 25\mu\text{m}$) was slowly added with stirring to 98% H_2SO_4 (17.5 ml) and stirred vigorously for at least 2 hours. 3g of KMnO_4 was then added as 0.15 (M) solution, slowly with continuous stirring for minimum 30 min with temperature controlled below 20°C , using ice. The stirring process was continued for another 30 min to arrest temperature hike. Sulphuric acid adds functional groups on graphite surface (functionalization) in the presence of reagent like KMnO_4 (oxidizer). Thick brownish black colloidal solution was obtained. 5 ml 30% H_2O_2 was added drop wise and stirred for another few minutes to convert graphite to graphene oxide and to destroy the excess KMnO_4 . However, the graphene oxide obtained contains traces of metal as impurity, which is eliminated by adding hydrochloric acid followed by repeated (at least 5 times) washing with de-ionized (DI) water (18 M Ω m). The blackish liquid turned into bright brownish yellow paste, which is pure graphene oxide (GO). To obtain graphene, GO has to be reduced. First GO is diluted with DI water at 1:10 wt. ratio and sonicated in an ultrasonic bath (Wensar WUC Series-12L) for 30 min, followed by drop-wise addition of hydrazine hydrate (20%) with constant stirring for 2 h. The liquid turned into black Graphene (or, Reduced Graphene oxide, rGO).

In the Hummers method, a combination of potassium permanganate (KMnO_4) and sulfuric acid (H_2SO_4) is used. Though permanganate is commonly used as oxidant (*e.g.*, de-hydroxylation), the active species is, in fact, di-manganese heptoxide (Mn_2O_7), generated in situ. The bimetallic heptoxide is far more reactive than its monometallic tetraoxide counterpart.

Functionalization of the synthesized sample

The synthesized rGO liquid was finally refluxed at 100°C for ~ 18 h to attach desired oxide species (like O_2^- , O^- , O^- etc.) on the surface. During prolonged reflux, condensation reactions are responsible for introduction of the desired functional groups which ultimately facilitate the gas sensing behavior by changing the resistivity/conductivity upon exposure to the analyte gas.

The sample was preserved as dispersed in DI water for future experiments and characterization.

Material characterizations

The phase identification of the synthesized GO was carried out by X-ray diffraction study (XRD; RIGAKU Ultima IV; Cu K_α reactor of wavelength 1.54 Å.) using graphene thin film deposited on 2.5 cm x 2.5 cm glass (silica) substrate by drop coating. Raman spectroscopy (Ranishaw

inVia.) with laser excitation wavelengths of 515 nm (2.41 eV) equipped with a notch filter with 50 cm^{-1} cutoff frequency was used to investigate the G-band as a function of thickness. For the measurement, graphene thin film was coated on polished glass substrate by spin coating. Fourier transformed IR studies were carried out on FTIR instrument (Shimadzu, IRA Infinity-1) using a $1.5\text{ cm} \times 1.5\text{ cm}$ thin film, deposited on a polished silica wafer <100> (which are transparent to IR). The aqueous suspension of exfoliated graphene sheets was dropped onto a polished silica (SiO_2) wafer substrate and characterized by an atomic force microscope (AFM; NT-MDT, Minus K Technology) in semi-contact mode to record the height profile and assess the layer thickness of the synthesized material. FESEM (SIGMA ZEISS) was used to observe the surface morphology and spreading of the drop coated thin film samples. For contact angle measurements, the rGO, functionalized rGO, GO and graphite samples were drop coated on cleaned glass substrates, dried at room temperature to make thin films and wettability was measured against water through contact angle study using Drop Shape Analyzer (KRÜSS GmbH – DSA25) instrument. Optical transmittance (T) was measured by UV-Visible Spectrophotometer (Perkin Elmer LAMBDA 25) as a function of wavelength in the range of 200–500 nm. Samples were also examined using a Tecnai G^2 30ST, 300 kV high resolution transmission electron microscope (HRTEM). For this, samples for measurement were prepared by dropping homogeneous dispersion onto a carbon-coated copper grid (200 mesh) at specific intervals and dried in the ambient conditions. Current-voltage (I/V) measurement was carried out using high resistance meter (HHV CMT 25, Keithley 6487 Voltage Source).

Sensor fabrication and measurements

For sensor fabrication, a small amount of liquid sample (1 ml) was diluted with DI water (5 ml) and ultrasonicated for minimum of ~ 30 min. to get a perfectly homogeneous dispersion. Simple Doctors' glass slide ($2.5\text{ cm} \times 2.5\text{ cm}$) cleaned with boiled DI water followed by acetone to avoid contaminations from impurities, was used as the substrate. Gold electrode (thickness $\sim 100\text{ nm}$) was deposited on the substrate by thermal evaporator (HHV AUTO 500) using a stainless steel mask. Two copper wires were attached by soldering with the gold electrodes, to measure the current output. Well dispersed graphene was drop coated on the substrate [displayed in Fig. 1 (a)], dried at room temperature to make it a conducting film for gas measurement studies. Substrates were placed on a heater (one-degree resolution of heating) and was closed with a Borosil glass beaker (volume $\sim 250\text{ ml}$) having two small holes at the top and side wall, to inject

the target gas and collect the exhausts, respectively [schematically represented in Fig. 1 (b)]. The substrate was heated to the desired temperature by the help of conduction heating method (temperature modulation has been calibrated using thermocouple) and after achieving stability, was exposed to the desired sensing gas and the change in resistance was recorded using Agilent Multimeter.

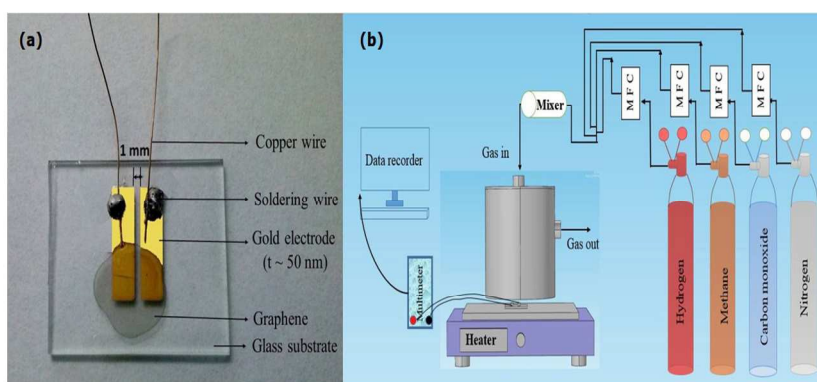


Fig. 1: (a) Real image of graphene sensor sample, drop coated on a glass substrate with attached Cu-wires. (b) Schematic diagram of gas measurement system.

Results and discussion

Characterization of graphite, graphene oxide (GO), graphene sheets (rGO) and functionalized rGO

Fig. 2 represents the x-ray diffraction patterns of graphite powder, graphene oxide and graphene sheets. Fig. 2(a) depicts the x-ray diffractogram of graphite (JCPDF, file no.: 75-2078) and Fig. 2(b) is the same of the procured graphite. The procured one is showing peak at 26.6° , which matches well with the JCPDF impressions and corresponds with $\langle 111 \rangle$ plane having interlayer spacing of 3.3 \AA . Fig. 2(c) is the XRD profile of graphene oxide (JCPDF, file no.: 82-2261) whereas, Fig. 2(d) is the same of the synthesized one. Two broad peaks at 9.7° and 12.4° of Fig. 2(d) indicate the nano-metric size and correspond with d_{111} (9.1 \AA) and d_{200} (7.1 \AA) planes, respectively. One much broader hump at 2θ value ranging between appx. $17.8\text{-}30.6^\circ$ [Fig. 2(d)] may be due to the tendency of reduction of GO to graphene while heating for drying. The d-spacing of graphene oxide increased to 7.1 \AA from 3.3 \AA of graphite powder, which is ascribed to the oxide-induced O-containing functional groups and inserted H_2O molecules⁹ that can be confirmed by further studies. These results suggest that the graphite powder has been completely

oxidized to GO. Fig. 2(e) represents the XRD pattern of synthesized reduced graphene oxide or, graphene. The Fig. shows one clear peak at 24.6° , the most prominent characteristic peak of graphene, indicating that the graphene oxide has been completely reduced to rGO. Peak at 24.6° corresponds to interlayer spacing of 3.6 \AA of d_{002} plane. Lattice strain was calculated using Williamson-Hall analysis¹² and found to be 0.26. The same for GO and graphite are 0.03 and 0.01, respectively (shown in Table I). The gradual escalation of lattice strain in the order $rGO > GO > Graphite$, indicates the introduction of defects within the lattice structure probably due to uneven epitaxial growth during synthesis, which ultimately benefits its application based on sensitivity.

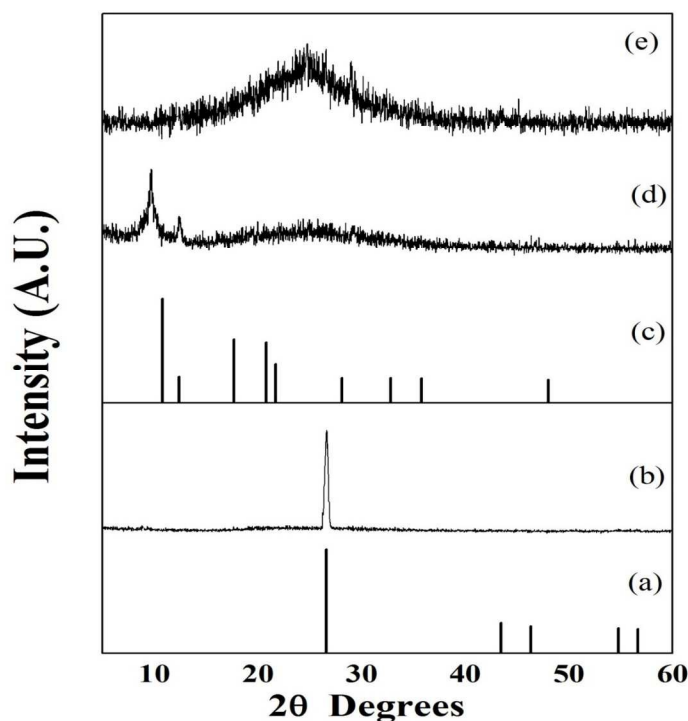


Fig. 2: X-ray diffractograms of (a) Graphite (JCPDF, file no.: 75-2078) (b) Procured graphite (BurGOyne Urbidges) (c) Graphene oxide (JCPDF, file no.:82-2261) (d) Synthesized graphene oxide and (e) Synthesized reduced graphene oxide or, graphene.

Fig. 3 shows the Raman spectra of GO, rGO and functionalized (refluxed) rGO taken at 515 nm LASER excitation (green LASER) along with the reference of bare glass (substrate) in the range of $500\text{--}2000 \text{ cm}^{-1}$. It is a powerful non-destructive tool to distinguish ordered and disordered crystal structures of carbon. Each of the de-convoluted Raman spectra shows two peaks; disorder-induced (D) band and tangential (G) band. G band is usually assigned to the E_{2g} phonon

of C sp^2 atoms, while D band is a breathing mode of κ -point phonons of A_{1g} symmetry.¹³ Two distinct peaks at ca. 1360 and 1608 cm^{-1} correspond with D and G band of GO whereas, the same at ca. 1345 and 1600 cm^{-1} correspond with those of rGO. On the other hand, the D and G band of functionalized rGO appear at ca. 1375 and 1615 cm^{-1} , respectively. There are some minor peak shifts of GO and functionalized rGO with respect to rGO probably caused by stress.¹⁴ However, the peak shifting for GO and functionalized rGO with respect to rGO are in the same direction indicating the presence of oxygen containing groups for both the species with respect to rGO. Intensity of both the bands of GO increases substantially, indicating the decrease in size of the in-plane sp^2 domains, possibly due to the extensive oxidation and ultrasonic exfoliation as, when the exfoliated GO is chemically reduced, the intensity of the D and G band increases further.¹⁵ This can be due to defects introduced during preparation procedure.¹⁴ The intense 'D' peak indicates that the graphene sheets have structural disorder. Increased intensity ratio of D and G band (I_D/I_G) in rGO (1.04) compared with GO (0.91) suggests a decrease in the average size of sp^2 domain due to the reduction process.

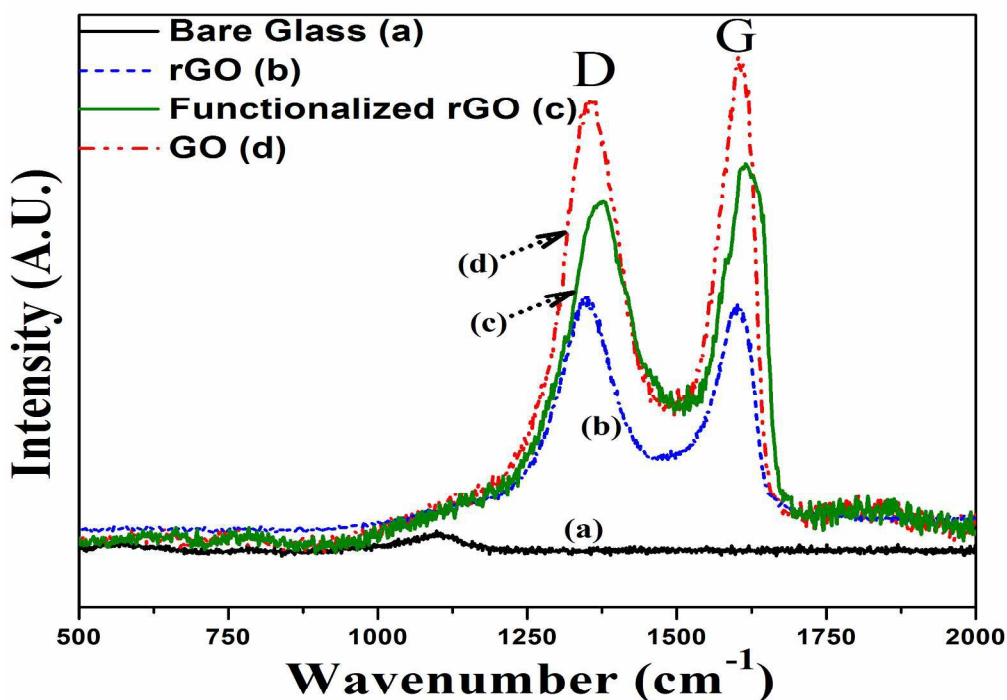


Fig. 3: Raman spectra of (a) Bare glass (used as the substrate of the samples) (b) Reduced graphene oxide (rGO), (c) Functionalized (refluxed) rGO and (d) Graphene oxide (GO).

The mean crystallite size (D_{RAMAN}) of GO, functionalized rGO and rGO layers were calculated using the following relation¹⁶

$$D_{\text{RAMAN}} = (2.4 \times 10^{-10}) \lambda_1^4 (I_D / I_G)^{-1} \dots \dots \dots (1)$$

Where, λ_1 is the LASER excitation wavelength (515 nm) and I_D/I_G is the intensity ratio of D and G bands. The mean crystallite size of rGO, functionalized rGO and GO calculated from the Raman peaks are given in Table I.

rGO, GO, functionalized (refluxed) rGO and graphite thin films were also used to test their wettability by measuring their static contact angle with water (shown in Fig. 4). It was found that the static contact angle between graphite film and water is 115° (Table-I). Because graphite consists of carbon atoms without any polarity, it demonstrates hydrophobic properties. For GO film and water, measured static contact angle is 46.5° , much less than 90° . Hence, GO shows a good hydrophilic property, as GO surface was presumably grafted with hydroxyl and epoxy groups. These polar groups change the graphite properties from hydrophobic to hydrophilic. After chemical reduction of GO by hydrazine hydrate, hydroxyl and epoxy groups are mostly eliminated, which is exhibited through the measured static contact angle of 138° which is larger than 90° .

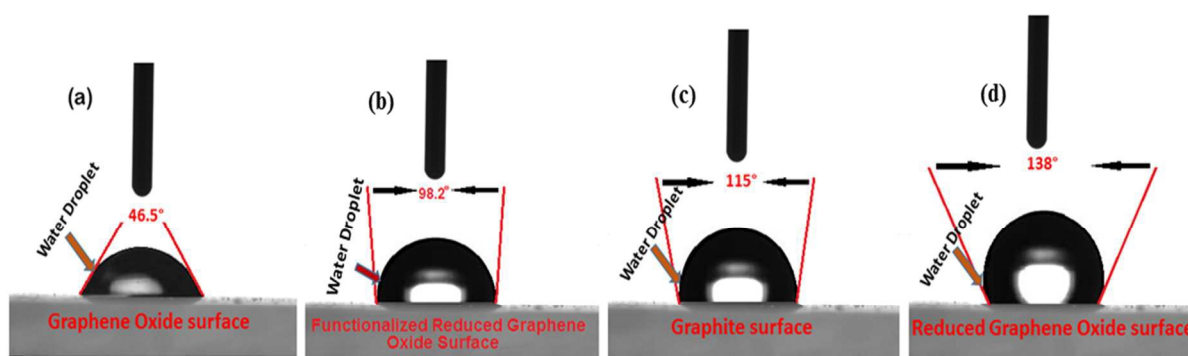


Fig. 4: Static contact angle measurement with water and (a) graphene oxide, (b) functionalized (refluxed) reduced graphene oxide (c) graphite and (d) reduced graphene oxide.

It is interesting to note that this contact angle is larger than that of graphite film and water. Even though isolated graphene also shows hydrophobic property, its degree of aqueous wettability is less than that of graphite. This can be understood easily as non-polarity of rGO is comparatively greater than graphite due to preferential reduction involving de-oxygenation and/or, de-hydroxylation during reduction by hydrazine hydrate. For this reason, graphite preserves more

oxygen containing functional groups than rGO. This can be further experimentally evidenced by FTIR analyses (provided later on). On the other hand, contact angle between functionalized rGO and water is 98.2° , which is also hydrophobic in nature but the hydrophobic tendency is much lower than rGO and graphite. Hence, from the experimental data we may conclude that wettability trend of these C-forms follow the order: GO > functionalized (refluxed) rGO > Graphite > rGO.

Reduced graphene oxide was characterized by FTIR in the mid-infrared range, and the results are shown in Fig. 5. The sharp peaks appearing at ca. 1050 and ca. 1389 cm^{-1} were characteristic peaks of $\nu_{\text{C-O}}$ and the $\delta_{\text{C-OH}}$ stretching vibrations, respectively.¹⁷ The peak at ca. 984 and 3441 cm^{-1} can be attributed to O–H stretching vibrations of adsorbed water molecules or interlayer water molecules and structural -OH groups. This particular peak is almost absent in rGO as, it is preferentially de-oxygenated or, de-hydroxylated during the reduction process by hydrazine hydrate. On the contrary, graphite shows this peak (at 3441 cm^{-1}) though, the magnitude is much less than that of GO or functionalized rGO. This de-oxygenation or, de-hydroxylation process of rGO is also confirmed by the wettability trend observed by the contact angle studies discussed earlier. In GO sample, the peak at ca. 1685 cm^{-1} can be attributed to O–H bending vibrations¹⁸⁻¹⁹ while, peak at ca. 1582 cm^{-1} reflects the skeletal vibration of GO.²⁰ The presence of oxygen or -OH indicates that during the oxidation process of the graphite powder with KMnO_4 in concentrated sulfuric acid medium, the original extended conjugated π -orbital system of graphite was destroyed and oxygen-containing functional groups were inserted into carbon skeleton *ie.*, the presence of these vibrations is indicative of the attachment of epoxide and hydroxyl groups. After reduction to rGO by hydrazine hydrate, these functional groups derived from the intensive oxidation have been eliminated (evidenced from Fig. 5). Disappearance of these two peaks (1582 and 1685 cm^{-1}) in rGO sample indicate that the graphene oxide (GO) have been successfully exfoliated to graphene sheets (rGO). However, some peaks especially those originating from -OH functional group (like, peaks at ca. 984 and/or, 3441 cm^{-1}) re-appear in the skeleton of functionalized rGO (by prolonged refluxing) indicating the presence of structural deformities, which ultimately facilitate the sensing performances.

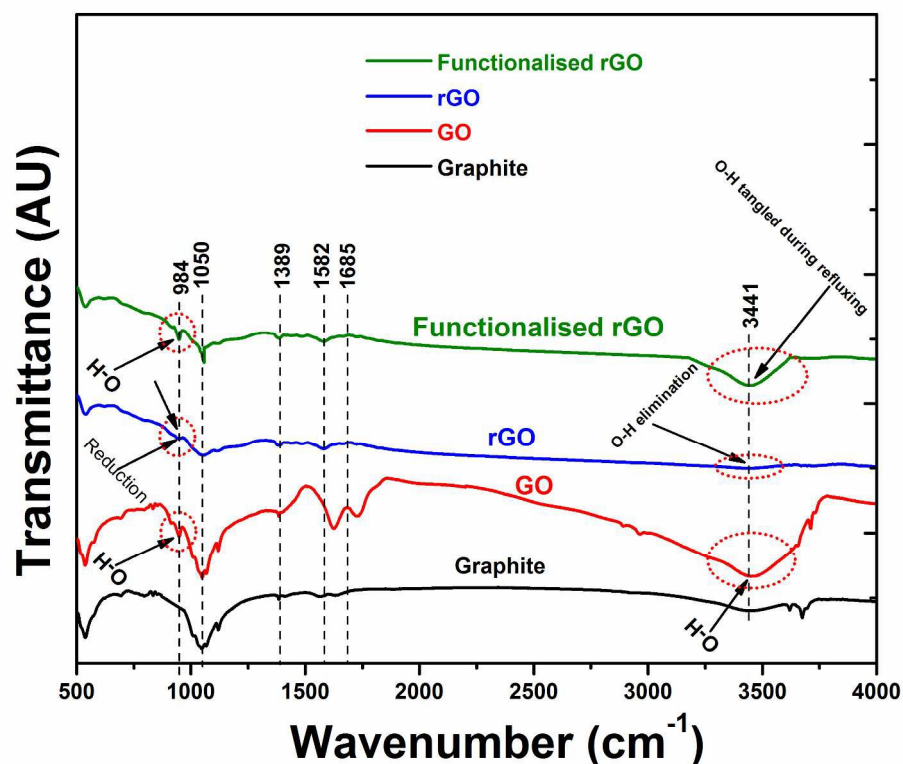


Fig. 5: FTIR spectra of graphite, graphene oxide (GO), reduced graphene oxide (rGO) and functionalized rGO (refluxed rGO).

A few representative TEM, HRTEM and related images of rGO thin films prepared by modified Hummers' method are presented in Fig. 6 (a-d). Fig. 6(a) and (b) depict the bright field images showing uniform thin layers in nano-metric dimension. Electron diffraction pattern is depicted in a selected area (SAED) suggesting the crystalline nature of the nanostructure [Fig. 6(c)]. The Fig. is indexed with $\langle 002 \rangle$ diffraction plane which corroborate well with Bragg's plane obtained from the XRD patterns and satisfy the reciprocal relationship between Miller indices (h, k, l planes) and SAED rings diameter.²¹ However, among the two techniques, the SAED technique is more authentic than X-ray diffraction because the dimensions of areas concerned are as small as several hundred nanometers whereas, X-ray diffraction deals with areas typically the samples' area, the dimensions of which is to be measured in several centimeters. The high-resolution transmission electron microscopic (HR-TEM) image of rGO is presented in Fig. 6(d) in which, those lattice planes (fringes) are visible that possess inter-planar

spacing greater than the lateral spatial resolution limits of the instrument. Here, the HR image displays a d-spacing value of 3.6 Å corresponding to the <002> crystal plane.

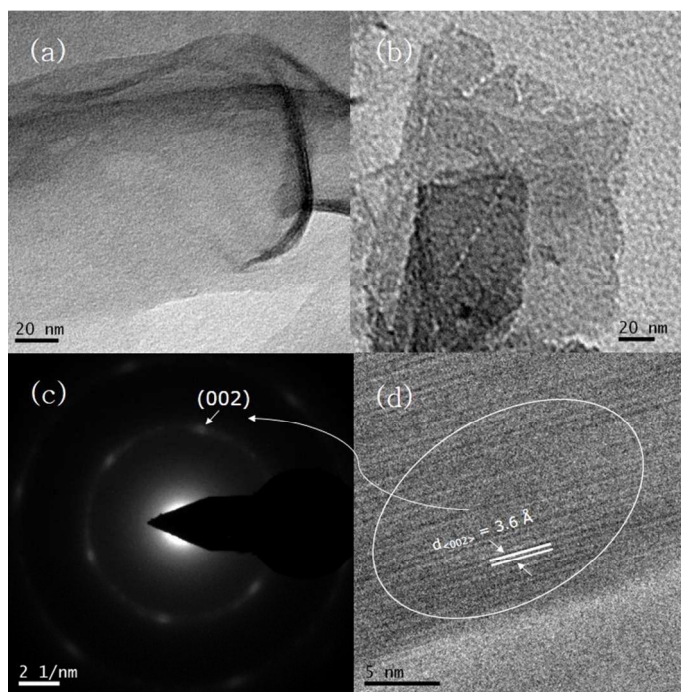


Fig. 6: (a) and (b) TEM micrograph of rGO (c) SAED patterns with indexed plane and (d) indexed fringes of HR-TEM image.

DC current-voltage (I/V) characteristics of as-fabricated graphene sensors at bias voltage ranging between -5 to +5 V at thirteen different operating temperatures between 30° C (room temperature) and 150° C (at 10° C intervals) were recorded in air with a high resistance meter and the I/V characteristic plots obtained, presented in Fig. 7. The I/V characteristic curves demonstrate a good ohmic behaviour, indicating that the metal-carbon junction between gold (Au electrode) and graphene and the carbon-carbon junction between graphene layers are both ohmic in nature. This is of prime significance as sensitivity of gas sensors can be maximized when these junctions are ohmic or have negligible junction resistance. Fig. 7 also shows that at a particular voltage, the current between the electrodes increases continuously with increase in temperature, which is the characteristic property of semiconductors and is very common in metal-semiconductor contact systems. The semiconducting behaviour of graphene is thought to originate from the polarization of adsorbed molecules (*e.g.*, water and oxygen sp.) and/or to

defects introduced into the graphene sheets during the preparation²² or even to the influence of the supporting substrate.²³

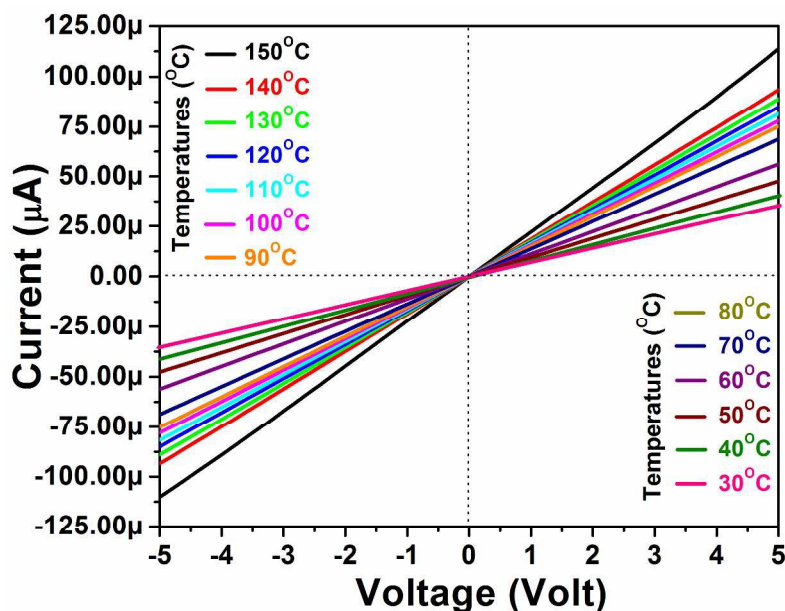


Fig. 7: Current Vs. Voltage (I-V) characteristic plots of graphene sensor films measured at temperatures between room temperature (30 °C) and 150 °C (at 10 °C intervals) in air.

In presence of oxidising or reducing gases, adsorbed species on the surface of graphene sheets acting as electron acceptor or donor, respectively. Thus, like many semiconducting gas sensors, sensitivity of gas sensors made of sheets of graphene, is also a surface phenomenon and charge transportation through adsorbed species is likely to be a function of sheet thickness and orientation with respect to ‘dirac point’ which is comparable with crystallite size²⁴ in polycrystallites. However further explorations to elucidate the transport mechanism in graphene film, have not been made in this study.

Sensitivity measurements of rGO film

Fig. 8 [(a), (b) & (c)] depicts the sensing characteristics of 18 h refluxed functionalized rGO films. Fig. 8 (a) exhibits the sensor response changes with respect to temperature (from room temperature upto 120 °C, at 30 °C intervals), in a 3D bar diagram format against different concentrations (10, 20 and 30 ppm) of carbon monoxide (CO) gas. It can be seen that with the increment of temperature, sensor response drops. Room temperature (29.6 °C) exposure of 30

ppm CO displays the maximum sensitivity of ~71%, which indicates that the sensor is best suited at room temperature. Without refluxing rGO film neither shows any room temperature sensitivity nor sensitivities at 60° and 90° C. It only shows 12%, 18% and 32% sensitivity against 10 ppm, 20 ppm and 30 ppm CO gas respectively, at 120° C temperature. Fig. 8 (b) and (c) demonstrate the dynamic response-recovery curves of functionalized graphene (rGO) sensor films against different concentrations of CO gas, measured at room temperature and elevated (120° C) temperature, respectively. The sensor signal showing p-type gas sensing behavior with 71%, 52% and 44% sensitivity at room temperature and 51%, 43% and 23% sensitivity at 120° C temperature, against 30 ppm, 20 ppm and 10 ppm CO gas exposure, respectively. Sensitivity at 60° and 90° C follow the intermediate trend (Table II). Fig. 8(b) and (c) also show that the sensor response increases with increasing concentration of the gas. After reaching a saturation plateau the dynamic curves switched from adsorption mode to desorption mode; these steady states (plateau) indicate saturation of gas molecules at the depletion regions as well as the response time of the sensors. The percent sensitivity or sensor response (S) of such p-type sensors was calculated using the following relation.²⁵

$$S = [(R_{\text{gas}} - R_{\text{air}}) / R_{\text{air}}] \times 100 \dots\dots\dots (2)$$

Where, 'R_{gas}' is the resistance in presence of target gas and 'R_{air}' is the same in air.

The response is quick (within 30 sec.) even to a trace amount (0.001% or, 10 ppm) of CO gas, however, the recovery is not so swift (>15 min) probably because of slow oxidation of gas molecules on the surface of the sensor films.

It has been observed that, the sensors are not able to recover 100% in normal way. However, the sensors may recover almost abundantly and come to their initial baseline value if exposed to UV-light, after removal of the target gas [Fig. 8(c)]. For UV exposure, the LED UV flashlight (385 nm) is exposed (LED-120 Inspection Light; Groz Engineering) during the recovery period for 1 min, when the CO gas is turned off; although the UV light does not speed up the recovery process. In this study, a number of experiments have been carried out to measure the sensitivity as a function of operating temperature and time. In all the cases, sensitivity of the sensor element showed approximately constant values, indicating the repeatability of the sensor.

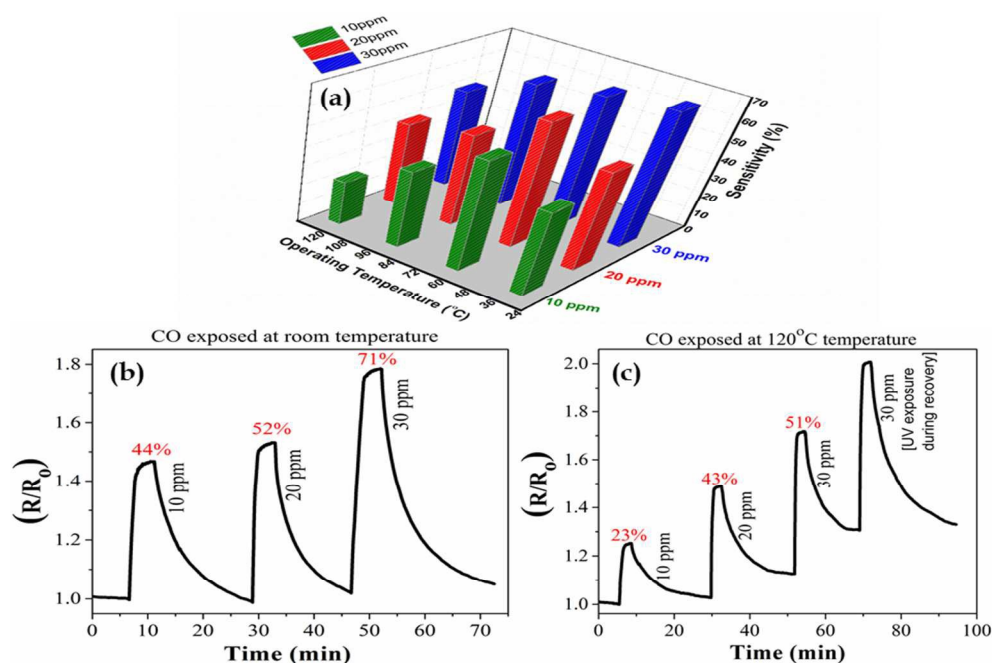


Fig. 8: (a) Sensor response of functionalized rGO film at different operating temperatures (from room temp. upto 120° C) against different concentrations of CO. (b) Dynamic response-recovery curves of functionalized rGO measured at room temperature against different concentrations of CO and (c) Dynamic response-recovery curves of functionalized rGO measured at elevated (120° C) temperature against CO gas of similar concentrations as of (b) (along with the response-recovery curve recovered by the help of short UV exposure).

Humidity effects on rGO film

Most of the gas sensors perform in humid atmospheric condition, hence in order to elucidate the role of humidity in the gas sensing properties of the rGO sensors, its responses towards water vapor were investigated at room temperature (30° C) as well as at elevated temperature (120° C). Fig. 9(a) and (b) exhibit the relative humidity (RH) effects on the prolonged refluxed rGO and without refluxing rGO films, respectively. It was found that the resistance changes (in terms of K Ohm) of the refluxed rGO film was only 15.75% at 120° C temperature [Fig. 9(a)], even in presence of excess humidity (as high as ~98% RH) and it became almost stable after a certain period of time which indicate that it is almost free from the interference of humidity. However,

the effect was slightly high (25.94%) at room temperature, which was fairly natural as, with temperature increment surface adsorbates (like H₂O) start disappearing. Influence of RH on without refluxed rGO was also investigated to compare the stability or shelf life period of both the films as, the presence of relative humidity is responsible for surface perturbation leading to adsorption-desorption-transformation of various species of oxygen including water molecules at the surface and interface regions. Fig. 9(b) shows that as the relative humidity gradually enhanced from 30% to 98% at room temperature, resistance of without refluxing rGO film (in M Ohm range) goes down continuously and there was no saturation plateau in the similar range of time interval as of Fig. 9(a), indicating that without refluxed rGO considerably affected by ambient moisture though, it does not show any room temperature sensitivity against gases. However, literature shows⁵ graphene film may sense water molecules but the effect reduces pretty well by introducing the reflux method, followed by a good shelf life period of such sensors.

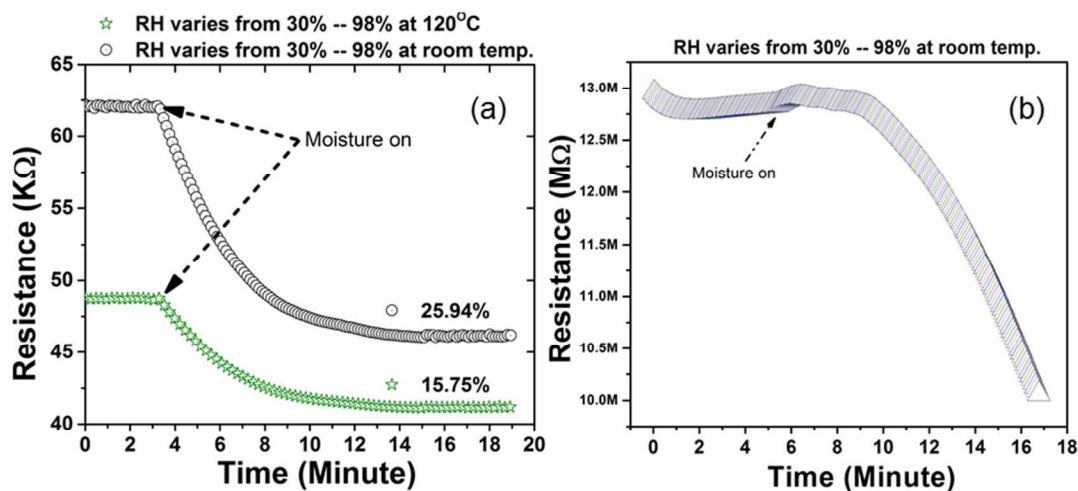


Fig. 9: Relative humidity effects (RH) on (a) the prolonged refluxed functionalized rGO [at room temperature and at elevated (120° C) temperature] (b) and without refluxing rGO

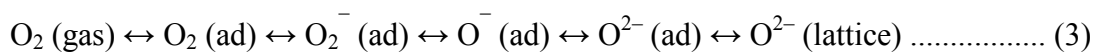
Selectivity tests of rGO film

To illuminate the selectivity, rGO films were also exposed against some other reducing gases like, methane (CH₄) and hydrogen (H₂) and ammonia (NH₃). The selectivity coefficient²⁶ $\beta = S_{CO}/S_{gas}$ (*i.e.*, the sensor response ratio between the target gas, CO and other gas) exhibits that $\beta =$

13.07 for CH₄, 8.23 for H₂ and 1.21 for NH₃ at the same operating temperature (120° C). The results (shown in Table II) confirm that the synthesized sensor is selective to CO gas with negligible cross sensitivity against very high concentrations (1000 ppm of CH₄ and H₂ each and 100 ppm of NH₃) compared to CO (maximum conc. of CO is only 30 ppm). Moreover, the sensor does not show any methane and/or hydrogen sensitivity at room temperature. The minimum temperature requirement to exhibit any sensor signal of such sensors is 100° C. However, the sensor shows room temperature sensitivity against 100 ppm ammonia, though the value is negligible (only 7% sensitivity) compared to the room temperature sensitivity against CO gas (71%). A comparison of CO sensing characteristics and device performances of different sensing materials already reported is presented in a tabular format (Table III)²⁷⁻³⁵ to compare and show the advancement and significance of the fabricated device made by functionalized rGO (presented at the end of Table III).

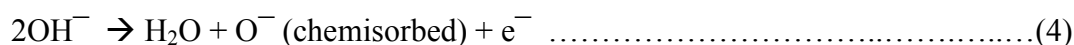
Sensing mechanism

The sensing mechanism involves surface conduction modulated by adsorbed gas molecules; electrical conductivity depends strongly on surface states produced by molecular adsorption, which result in space-charge layer changes and band modulation. On the surface of the sensor materials, two types of adsorption can occur: physisorption, the first step of the association of the gas species with the sensor surface, and chemisorption, which involves exchange of electrons between the adsorbed species and the material surface. The major difference between these two processes is that physisorption is exothermic while chemisorption is endothermic.³⁶ The sensing characteristics are widely considered to be related with chemisorbed oxygen species, water and/or hydroxyl ions, which can act as intermediates, catalyzing the charge transfer processes between gas species and the film and is responsible for the study of gas sensing mechanisms (Fig. 10). The adsorbed oxygen on the surface can be of several forms: O₂, O₂⁻, O⁻ and O²⁻. Of these species, O₂ is quite inactive because its activation energy is high; its concentration is also very low. If reducing agent (like, CO) is introduced, the O⁻ disappears very quickly relative to O₂⁻, indicating higher activity of O⁻ than O₂⁻. The lattice oxygen, O²⁻ can also be reactive with the incoming reducing agent. It has been proposed that adsorbed oxygen changes to various oxygen anionic species, transferring an electron from rGO to the chemisorbed oxygen according to the following processes³⁷:



Where, CO acts as a donor molecule (n-type donor) (Fig. 10) with charge transfer capacity of 0.012 eV³⁸ and makes rGO to behave as p-type; oxygen groups in defected rGO are responsible for reactions with C–O bond of CO gas molecules.

In this study, The prolonged reflux method helped to attach hydroxyl groups (–OH) into the reduced graphene oxide skeleton which ultimately increases the number of electrons in the conduction band leading to an augmented depletion layer. The attached OH[–] is responsible for generation of oxygen ion (O[–]) which remains chemisorbed on the surface of the material and gradually transforms into some other forms of anionic oxygen (like, O⁼) by extracting free electrons from the conduction band, resulting in an electron depleted surface layer and a consequent rise in resistance. The relevant chemical species exist in equilibrium³⁹⁻⁴¹ as follows:



When the sensor film surface is exposed to the analyte gas (like CO), it gets physisorbed:



and the probable ways of decomposition of such analytes on the sensor surface may be considered as⁴²⁻⁴³:



The processes indicate the in-situ generation of atomic/ionic oxygen, which makes the process irreversible in nature. These chemisorbed charged oxygen species at the grain boundaries are responsible for the space charge appearance and band modulation. Therefore, the variation of the chemisorbed molecule density is supposed to be the main factor responsible for the electrical response whereas the rGO phase remains chemically stable. For this reason, such sensors can be used repeatedly and has prolonged shelf-life (unless humidity or other external interfering agents affect the sensor surface).

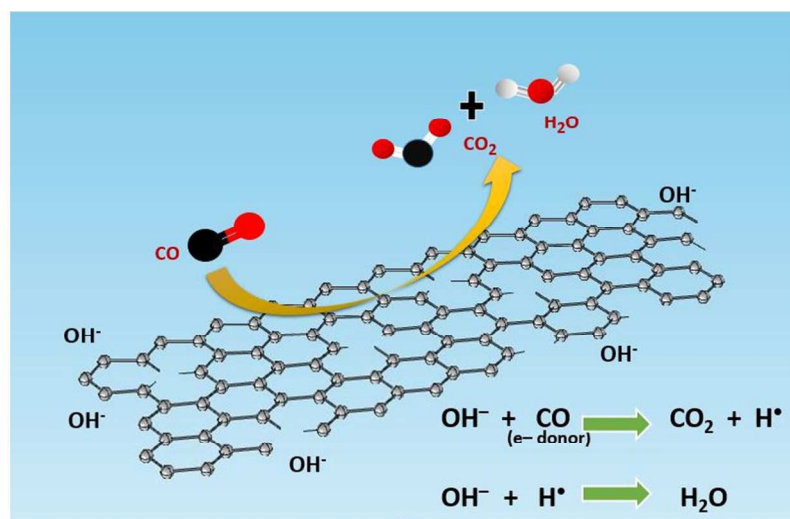


Fig. 10: Schematic representation of gas sensing mechanism of CO adsorption on graphene surface (carbon atom in black, oxygen in red and hydrogen atom in white).

In the decomposition reactions of analyte gases in presence of surface adsorbates, the resultant products are carbon dioxide (CO₂) and water (H₂O) though the reaction proceeds through several intermediates. These reactions decrease device conductivity as a function of time⁴⁴ and hence increase the resistance (p-type behavior) of the device prototype. As conductivity is proportional to the product of charge-carrier density and mobility, it is evident that changes in the number density or mobility of carriers, or both, must be responsible for the change in conductivity.⁴⁵ Graphene's linear band structure around the Dirac points (the six κ points in the Brillouin zone) is responsible for the gas adsorption, which possibly increase the number of electrons as the gas is a donor one. Closed-shell adsorbates such as CO do not directly change the band structure of graphene, but rather alter the distribution of charges within graphene.⁴⁶ Adsorbed water is a

prevalent surface “impurity”, especially when located between the graphene and the substrate, which can shift the impurity bands of the substrate in the vicinity of graphene’s Fermi level and so cause indirect doping of the graphene. Indeed, even if not initially present between the graphene and substrate, water molecules might diffuse into this region upon exposure to humid air.⁴⁷ Recent theoretical studies also support this conclusion by demonstrating that gas molecules adsorb only weakly on pristine graphene, but adsorb more strongly on defective graphene (*i.e.*, graphene that contains a vacancy due to point defect or incomplete removal of epoxy/oxygenated functional groups, that may generate during the reduction process or attachment of desired functional groups by prolonged condensation reaction through reflux method) surface.^{48,9} These defects and foreign functional groups remarkably affect the electronic conductivity of graphene based devices like gas sensors. The relative position of HOMO and LUMO of the adsorbate CO molecule with respect to Dirac point in graphene is presented in Fig. 11, which determines the direction of charge transfer.

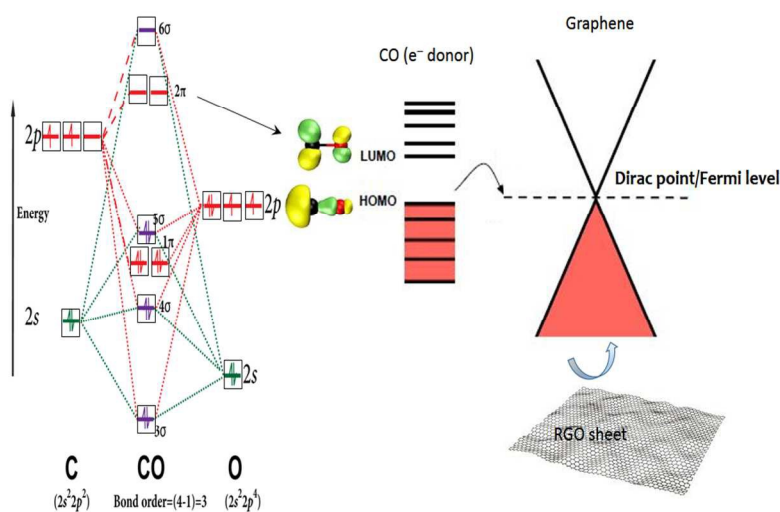


Fig. 11: The relative position of HOMO and LUMO of the adsorbate CO molecule with respect to Dirac point in graphene (C atom in black and O atom in red).

Usually CO molecule acts as a donor but the sites of the charge transfer only depends on the orientation of the molecules with respect to the surface. The differences in charge transfer are due to differences in orbital overlap between the HOMO (5σ ; weakly antibonding) of the CO molecule and graphene. The LUMO (2π ; strongly antibonding symmetry) seems to play no

important role in the electron doping process although it is closer to the Dirac point than the HOMO. In this case, HOMO is thus the more important orbital and confers transferability of charge to graphene. Because the HOMO is mainly located on the C atom, the charge transfer is largest when the C atom is closest to the surface, smallest when the O atom is closer to the surface, and intermediate when both atoms are at (almost) equal distance from the surface. Graphene also exhibits dangling edge-bonds during CO adsorption.⁴⁹ However, such edge effects, though providing energetically favourable sites for gas absorption, contribute only to a small extent (~2%) of the total electrical response of a typical microscale graphene device.⁵⁰ Stronger adsorption arises from either defects or doping with suitable components.⁴⁸

Conclusion

Graphene or reduced graphene oxide can be synthesized with added functional groups through wet chemical bottom up approach (modified Hummers' method), with graphene oxide as the intermediate product. This material (graphene) possesses high conductivities that can undergo measurable changes in terms of conductivity/resistivity when exposed to CO gas and produces an electrical signal with a magnitude proportional to the concentration of the analyte gas. Gas sensing experiments exhibit about 71% sensitivity at room temperature against 30 ppm CO with negligible cross sensitivity against other reducing gases like NH₃, CH₄ and H₂. Graphene is thus a highly potential material for development of CO gas sensor with high degree of sensitivity, selectivity and reliability proving it selective to CO gas at room temperature within permissible exposure limits.

Supporting Information

AFM image of a multilayer graphene flake with height profile; FESEM micrograph of RGO; UV-Visible spectra.

Acknowledgement

Authors acknowledge the financial support from Ministry of New and Renewable Energy (MNRE) and Department of Science & Technology (DST), Govt. of India. Authors also acknowledges Prof. Partha Chaudhuri, IACS, Kolkata, for assistance in recording the RAMAN spectra. DP is indebted to DST-CSIR Sensor Hub (Grant no. GAP 0332).

Notes and references

1. K. S. Novoselov, A. K. Geim, S.V. Morozov, D. Jiang, Y. Zhang, S. V. Dubonos, I. V. Grigorieva, A. A. Firsov, *Science*, 2004, **306**, 666-669.
2. S. Das, M. Kim, J-W. Lee, W. Choi, *Critical Reviews in Solid State and Materials Sciences*, 2014, **39**, 231-252.
3. S. Majumdar, P. Nag, P. S. Devi, *Mater. Chem. Phys.*, 2014, **147**, 79–85.
4. S. Majumdar, *Appl. Surf. Sci.*, 2016, **376**, 290–297.
5. F. Schedin, A. K. Geim, S. V. Morozov, E. W. Hill, P. Blake, M. I. Katsnelson, K. S. Novoselov, *Nat. Mater.*, 2007, **6**, 652–655.
6. Z. Chen, A. Umar, S. Wang, Y. Wang, T. Tian, Y. Shang, Y. Fan, Q. Qi, D. Xu, L. Jiang, *Nanoscale*, 2015, **7**, 10259-10266.
7. W. Chen, F. Li, P. C. Ooi, Y. Ye, T. W. Kim, T. Guo, *Sens. Actuators B*, 2016, **222**, 763–768.
8. S. Wang, Z. Chen, A. Umar, Y. Wang, T. Tian, Y. Shang, Y. Fan, Q. Qi, D. Xu, *J. Phys. Chem. C*, 2015, **119**, 28640–28647.
9. T. Wang, D. Huang, Z. Yang, S. Xu, G. He, X. Li, N. Hu, G. Yin, D. He, L. Zhang, *Nano-Micro Letters*, 2016, **8(2)**, 95-119.
10. C. Yi, *Dissertation submitted for the degree of Doctor of Philosophy*, Department of Electrical and Computer Engineering, Graduate School of Duke University, Durham NC, USA, 2013.
11. I. Blumenthal, *J. Royal Soc. Med.*, 2001, **94**, 270-272.
12. V. D. Mote, Y. Purushotham, B. N. Dole, *J. Theor. Appl. Phys.*, 2012, **6(6)**, 1-8.
13. F. Tuinstra, J. L. Koenig, *J. Chem. Phys.*, 1970, **53**, 1126–1130.
14. Z. H. Ni, H. M. Wang, Y. Ma, J. Kasim, Y. H. Wu, Z. X. Shen, *ACS Nano*, 2008, **2**, 1033–1039.
15. S. Stankovich, D. A. Dikin, R. D. Piner, K. A. Kohlhaas, A. Kleinhammes, Y. Y. Jia, Y. Wu, S. T. Nguyen, R. S. Ruoff, *Carbon*, 2007, **45**, 1558–1565.
16. L. G. Cançado, K. Takai, T. Enoki, M. Endo, Y. A. Kim, H. Mizusaki, A. Jorio, L. N. Coelho, R. Magalhães-Paniago, M. A. Pimenta, *Appl. Phys. Lett.*, 2006, **88**, 163106–163106-3.
17. C. T. G. Smith, R. W. Rhodes, M. J. Beliatas, K. D. G. Imalka Jayawardena, L. J. Rozanski, C. A. Mills, S. R. P. Silva, *Appl. Phys. Lett.*, 2014, **105(7)**, 073304–073304-5.
18. T. Szabó, O. Berkesi, I. Dékány, *Carbon*, 2005, **43**, 3186-3189.
19. C. Hontoria-Lucas, A. J. López-Peinado, J. D. López-González, M. L. Rojas-Cervantes, R. M. Martín-Aranda, *Carbon*, 1995, **33(11)**, 1585-1592.
20. P. Guo, H. Song, X. Chen, *Electrochem. Comm.*, 2009, **11**, 1320–1324.
21. P. E. Batson, N. Dellby, O. L. Krivanek, *Nature*, 2002, **418**, 270–273.
22. K. Kim, H. J. Park, B. C. Woo, K. J. Kim, G. T. Kim, W. S. Yun, *Nano Lett.*, 2008, **8(10)**, 3092-3096.
23. S. Fratini, F. Guinea, *Phys. Rev. B*, 2008, **77**, 195415–195415-6.
24. C. Go´mez-Navarro, R. T. Weitz, A. M. Bittner, M. Scolari, A. Mews, M. Burghard, K. Kern, *Nano Lett.*, 2007, **7(11)**, 3499–3503.

25. S. Majumdar, *Ceram. Int.*, 2015, **41**, 14350–14358.
26. P. Nag, S. Majumdar, A. Bumajdad, P. S. Devi, *RSC Adv.*, 2014, **4**, 18512–18521.
27. K. K. Bhargav, S. Ram, S. B. Majumder, *J. Mater. Sci.*, 2015, **50**, 644–651.
28. N. Barsan, U. Weimar, *J. Phys.: Condens. Matter*, 2003, **15**, R813–R839.
29. S. Antonaroli, B. Crociani, C. D. Natale, S. Nardis, M. Stefanelli, R. Paolesse, *Sens. Actuators B*, 2015, **208**, 334–338.
30. H. Yamaura, T. Jinkawa, J. Tamaki, K. Moriya, N. Miura, N. Yamazoe, *Sens. Actuators B*, 1996, **35-36**, 325–332.
31. Z. M. Ao, J. Yang, S. Li, Q. Jiang, *Chem. Phys. Lett.*, 2008, **461**, 276–279.
32. J. F. Chang, H. H. Kuo, I. C. Leu, M. H. Hon, *Sens. Actuators B*, 2002, **84**, 258–264.
33. J. T. McCue, J. Y. Ying, *Chem. Mater.*, 2007, **19**, 1009–1015.
34. J. H. Yu, G. M. Choi, *Sens. Actuators B*, 2001, **75**, 56–61.
35. A. Maity, A. Ghosh, S. B. Majumder, *Sens. Actuators B*, 2016, **225**, 128–140.
36. J. Xiao, S. Sitamraju, M. J. Janik, *Langmuir*, 2014, **30(7)**, 1837–1844.
37. A. Prakash, S. Majumdar, P. S. Devi, A. Sen, *J. Membrane Sci.*, 2009, **326**, 388–391.
38. X. Li, H. Wang, J. T. Robinson, H. Sanchez, G. Diankov, H. Dai, *J. Am. Chem. Soc.*, 2009, **131**, 15939–15944.
39. S. Banerjee, P. Nag, S. Majumdar, P. S. Devi, *Mater. Res. Bull.*, 2015, **65**, 216–223.
40. S. Chakraborty, I. Mandal, I. Ray, S. Majumdar, A. Sen, H. S. Maiti, *Sens. Actuators B*, 2007, **127**, 554–558.
41. S. Majumdar, P. S. Devi, *AIP Conf. Proc.*, 2010, **1276(1)**, 1–7.
42. S. Majumdar, A. Nandi, S. K. Datta, H. Saha, *IEEE Xplore*, 2016, 162–166. (<http://dx.doi.org/10.1109/CMI.2016.7413731>).
43. I. Ray, S. Chakraborty, A. Chowdhury, S. Majumdar, A. Prakash, R. Pyare, A. Sen, *Sens. Actuators B*, 2008, **130**, 882–888.
44. J. D. Fowler, M. J. Allen, V. C. Tung, Y. Yang, R. B. Kaner, B. H. Weiller, *ACS Nano*, 2009, **3(2)**, 301–306.
45. T. O. Wehling, M. I. Katsnelson, A. I. Lichtenstein, *Chem. Phys. Lett.*, 2009, **476**, 125–134.
46. W. Choi, J-W. Lee, *Graphene Synthesis and Applications*, CRC Press, Taylor & Francis Group, Boca Raton, FL, 2012.
47. Z. M. Ao, J. Yang, S. Li, Q. Jiang, *Chem. Phys. Lett.*, 2008, **461**, 276–279.
48. Y. H. Zhang, Y. B. Chen, K. G. Zhou, C. H. Liu, J. Zeng, H. L. Zhang, Y. Peng, *Nanotechnol.*, 2009, **20**, 185504–185504-8.
49. B. Huang, Z. Y. Li, Z. R. Liu, G. Zhou, S. G. Hao, J. Wu, B. L. Gu, W. H. Duan, *J. Phys. Chem. C*, 2008, **112**, 13442–13446.
50. H. E. Romero, P. Joshi, A. K. Gupta, H. R. Gutierrez, M. W. Cole, S. A. Tadigadapa, P. C. Eklund, *Nanotechnol.*, 2009, **20**, 45501–245501-8.

Table captions

Table I: Some physical properties of different carbon components (Graphene, Graphene oxide and Graphite).

Table II: Sensor response of functionalized rGO film at different temperatures against different gases at diverse concentrations.

Table III: Comparison of CO sensing characteristics of different sensing materials.

Fig. captions

Fig. 1: (a) Real image of graphene sensor sample, drop coated on a glass substrate with attached Cu-wires. (b) Schematic diagram of gas measurement system.

Fig. 2: X-ray diffractograms of (a) Graphite (JCPDF, file no.: 75-2078) (b) Procured graphite (BurGOyne Urbidges) (c) Graphene oxide (JCPDF, file no.:82-2261) (d) Synthesized graphene oxide and (e) Synthesized reduced graphene oxide or, graphene.

Fig. 3: Raman spectra of (a) Bare glass (used as the substrate of the samples) (b) Reduced graphene oxide (rGO), (c) Functionalized (refluxed) rGO and (d) Graphene oxide (GO).

Fig. 4: Static contact angle measurement with water and (a) graphene oxide, (b) functionalized (refluxed) reduced graphene oxide (c) graphite and (d) reduced graphene oxide.

Fig. 5: FTIR spectra of graphite, graphene oxide (GO), reduced graphene oxide (rGO) and functionalized rGO (refluxed rGO).

Fig. 6: (a) and (b) TEM micrograph of rGO (c) SAED patterns with indexed plane and (d) indexed fringes of HR-TEM image.

Fig. 7: Current Vs. Voltage (I-V) characteristic plots of graphene sensor films measured at temperatures between room temperature (30 ° C) and 150° C (at 10° C intervals) in air.

Fig. 8: (a) Sensor response of functionalized rGO film at different operating temperatures (from room temp. upto 120o C) against different concentrations of CO. (b) Dynamic response-recovery curves of functionalized rGO measured at room temperature against different concentrations of CO and (c) Dynamic response-recovery curves of functionalized rGO measured at elevated (120o C) temperature against CO gas of similar concentrations as of (b) (along with the response-recovery curve recovered by the help of short UV exposure).

Fig. 9: Relative humidity effects (RH) on (a) the prolonged refluxed functionalized rGO [at room temperature and at elevated (120° C) temperature] (b) and without refluxing rGO films.

Fig. 10: Schematic representation of gas sensing mechanism of CO adsorption on graphene surface (carbon atom in black, oxygen in red and hydrogen atom in white).

Fig. 11: The relative position of HOMO and LUMO of the adsorbate CO molecule with respect to Dirac point in graphene (C atom in black and O atom in red).

Table I: Some Physical Properties of Different Carbon Components (Graphene, Graphene oxide and Graphite)

Samples	Contact angle (degree)	Crystallite size from RAMAN D_{RAMAN} (nm)	Lattice strain calculated from XRD
Graphene or, Reduced Graphene Oxide (rGO)	138	16	0.26
Graphene Oxide (GO)	46.5	18	0.03
Graphite	115	–	0.01
Functionalized (refluxed) rGO	98.2	19	–

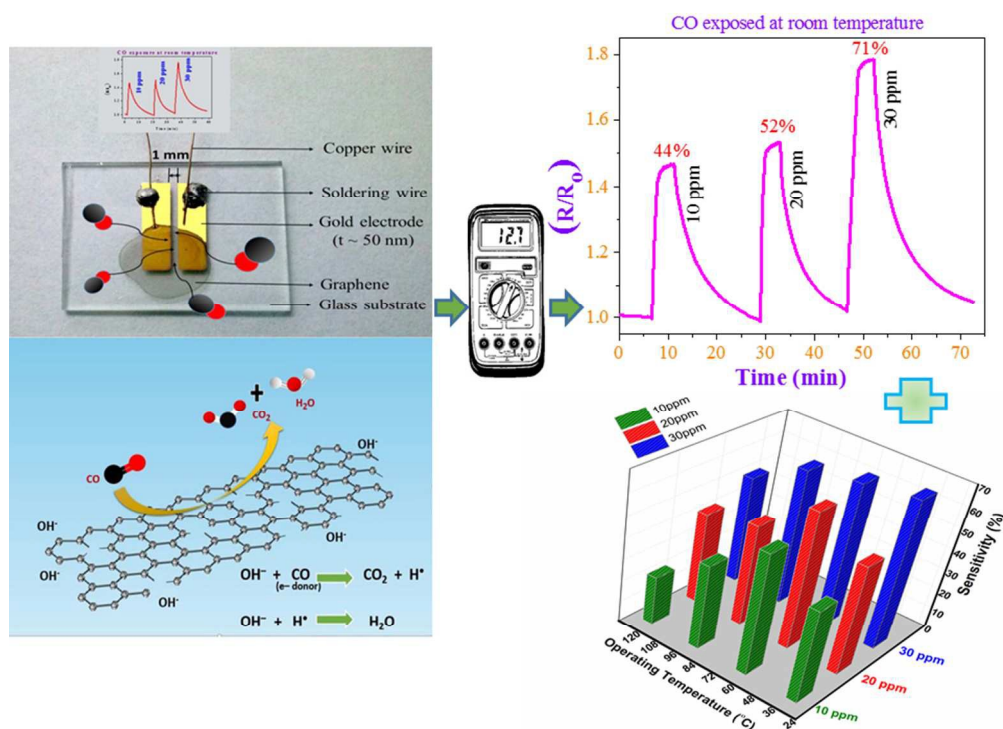
Table II: Sensor response of functionalized rGO Film at Different Temperatures Against Different Gases at Diverse Concentrations

Temperature	Sensor Response (%S)					
	30 ppm CO	20 ppm CO	10 ppm CO	100 ppm NH ₃	1000 ppm CH ₄	1000 ppm H ₂
Room Temperature (RT)	71	52	44	7	*ND	*ND
60° C	68	65	57	15	*ND	*ND
90° C	64	48	40	28	*ND	*ND
100° C	60	45	35	33	3.1	5.6
120° C	51	43	23	42	3.9	6.2

*ND: Not Detectable

Table III. Comparison of CO Sensing Characteristics of Different Sensing Materials

Sl. No.	Material(s) sensing CO gas	Sensing parameter(s)	Selectivity to CO	Ref.
1.	Nano-crystalline LaFeO ₃ and LaFe _{0.8} Co _{0.2} O ₃ particles	Sensitivity measured against 100 ppm CO.	Selective to CO at 100° C operating temperature	27
2.	Pd doped SnO ₂	Sensitivity measured in presence of humidity in the temperature range between 200 and 400° C.	Selectivity tests not performed	28
3.	Nanogravimetric sensors made by [Pd(η^2 -ol)(8-(di-tert-butylphosphinoxy)quinoline)] and [Pd(η^2 -ol)(8-(di-tert-butylphosphinoxy)-2-methylquinoline)]	Sensitivity measured against 125 and 250 ppm CO.	[Pd(η^2 -ol)(8-(di-tert-butylphosphinoxy)quinoline)] is selective to CO, even in presence of humidity.	29
4.	Rb ₂ CO ₃ promoted In ₂ O ₃	Responds well to 200-4000 ppm CO in wet air at 300° C and exhibits low cross sensitivities to H ₂ , CH ₄ , C ₃ H ₆ , NO and CO ₂ .	Selective to CO at elevated temperature (200-300° C)	30
5.	Al doped graphene	CO sensitivity enhancement shown via introducing large amount of shallow acceptor states by forming Al-CO bond.	Selectivity tests not performed	31
6.	Al-doped ZnO films deposited onto SiO ₂ /Si substrates	Maximum sensitivity of 61.6% reported for 65 nm ZnO:Al film thickness at the operating temperature of 400° C. Sensitivity and response time improved by increasing the operating temperature.	Selectivity tests not performed	32
7.	Au- and Pt-doped SnO ₂ -In ₂ O ₃ nanocomposites	Showed superb sensitivity for both reducing and oxidizing gases like CO, NO and NO ₂ .	Not selective to CO	33
8.	CuO- and ZnO-doped pellet-type SnO ₂	Sensitivity measured for 200 ppm CO and 200 ppm H ₂ in the temperature range 80 to 450° C.	Showed high selectivity to CO at elevated (~160° C) operating temperature.	34
9.	25% NiFe ₂ O ₄ -75% La _{0.8} Pb _{0.2} Fe _{0.8} Co _{0.2} O ₃ composite nano-powders	Exhibits excellent sensitivity toward CO at operating temperatures between 125 and 175° C.	Selective to 250 ppm CO at ~175° C operating temperature in presence of other gases like, 500 ppm C ₄ H ₁₀ , 500 ppm H ₂ and 5 ppm NO ₂ .	35
10	Functionalized (18 h refluxed at 100° C) reduced graphene oxide (rGO)	Showed the highest sensitivity (~71%) against 30 ppm CO at room temperature. Sensitivity decreases with increasing operating temperature.	Selective to CO. Other n-type reducing gases (like, 100 ppm ammonia, 1000 ppm methane and 1000 ppm hydrogen) showed negligible sensitivity compared to CO.	<i>Present Study</i>



Graphical Abstract
254x190mm (96 x 96 DPI)